AIP Advances

Enhancement of harvesting capability of coupled nonlinear energy harvesters through high energy orbits

P. V. Malaji (iD), M. I. Friswell (iD), S. Adhikari (iD), and G. Litak (iD)

View Online   Export Citation   CrossMark

ARTICLES YOU MAY BE INTERESTED IN

Enhancement of harvesting capability of coupled nonlinear energy harvesters through high energy orbits

View Online   Export Citation   CrossMark

P. V. Malaji,[1,a] (iD) M. I. Friswell,[2,b] (iD) S. Adhikari,[2,c] (iD) and G. Litak[3,d] (iD)

AFFILIATIONS

[1] BLDEA's V. P. Dr. P. G. Halakatti College of Engineering and Technology, Vijayapur 586101, India
[2] College of Engineering, Swansea University, Swansea SA1 8EN, United Kingdom
[3] Lublin University of Technology, Nadbystrzycka 36, PL-20-618 Lublin, Poland

[a] Electronic mail: pradeepmalaji@bldeacet.ac.in
[b] Author to whom correspondence should be addressed: m.i.friswell@swansea.ac.uk
[c] Electronic mail: s.adhikari@swansea.ac.uk
[d] Electronic mail: g.litak@pollub.pl

ABSTRACT

Mechanical coupling in similar energy harvesters has the potential to enhance their broadband harvesting capability. However, often the performance of one harvester dominates the other, and the coupling transfers energy from the high frequency harvester to the low frequency harvester, thus reducing the capability of the high frequency harvester. Hence, researchers have proposed using the high frequency harvester only as an auxiliary oscillator to save the material cost. This paper investigates the possibility of enhancing the energy harvesting capability of both coupled harvesters. A torsionally coupled electromagnetic pendulum harvester system is considered, which is suitable for low frequency (<5 Hz) applications. The harmonic balance method is used to identify possible multiple solutions, and high magnitude solutions are observed to coexist with low magnitude solutions. These high energy solutions, which are often missed in the numerical simulation, can be attained by a careful choice of initial conditions or energy input. The simulation results show that more energy can be harvested over a wider range of frequencies by ensuring that the response occurs in the high energy orbits. The results show an enhancement of the bandwidth by 54% and 140% for the low and high frequency harvesters, respectively, with the optimum initial conditions. Moreover, an isolated frequency island is reported, which occurs due to the coupling of the nonlinear harvesters.

The ambient environment contains many vibration sources, such as human motion, vehicles, ocean waves, and wind. Useful electrical energy can be harvested from such vibration sources via suitable transduction methods (piezoelectric, electromagnetic, and electrostatic).[1-3] This harvested electrical energy can solve the issue of powering wireless sensors. Conventional linear harvesters work in a narrow range of frequencies and hence are inappropriate for practical applications as most excitation sources have broadband vibration characteristics.[4] To overcome this limitation, many researchers are focusing on nonlinear harvesters that can harvest broadband energy[2,5-10] and multiple/multi-frequency harvesters, where a set of harvesters or multi-degree of freedom systems are used for broadband harvesting.[11-15]

A set of linear harvesters with different tip masses were analyzed theoretically and experimentally by Ferrari et al.[16] for broadband energy harvesting. They considered a set of harvesters with different natural frequencies, which can produce power over a wider bandwidth. This kind of system requires more space and the power generated also is less.[17] A harvesting system with fewer harvesters and coupling has been proposed for broadband harvesting. Malaji and Ali[18] proposed coupled and grounded multiple pendulum harvesters to enhance the harvester performance. A nonlinear

piezoelectric energy harvester with a magnetic oscillator was proposed by Tang and Yang.[19] They reported an enhanced response amplitude and bandwidth of the harvester with a lower natural frequency than the auxiliary oscillator. Similar work with electromagnetic transduction was demonstrated by Zergoune et al.,[20] who considered harvesting from both harvesters with weak magnetic coupling. They reported that the energy localization phenomenon due to mistuning leads the low frequency harvester response to dominate the high frequency harvester in terms of the power output. They suggested harvesting only from the lower frequency harvester to save material, although the analysis of the frequency bandwidth was not considered. Similar results were observed by Zhou et al. and Masaaki et al.[21,22]

The above research has demonstrated that the coupling between the harvesters with different natural frequencies leads to an energy transfer from the harvester with higher natural frequency to the harvester with a lower natural frequency. This leads to the performance enhancement of only one harvester, whereas the other harvester has a negligible contribution. If the harvesters are nonlinear, coupling them will lead to complex dynamics with multiple solutions and high and low energy orbits. This paper explores the possibilities of operating both the harvesters at high energy orbits over a wide frequency band with an additional energy supply to the harvesters via different initial conditions, and hence enhancing the performance of both the harvesters.

The mathematical model of the harvesting system with torsionally coupled pendulums is now considered. Figure 1(a) shows the electro-mechanical system with two pendulums of different lengths, l_1 and l_2. These pendulums are pivoted to the shafts of the electromagnetic generators with rotating magnets (rotor) and fixed coil windings (stator). When a pendulum oscillates, a current, I, is generated due to electromagnetic induction, as shown in Fig. 1(b). These pendulums are coupled using an elastic torsional spring, k.
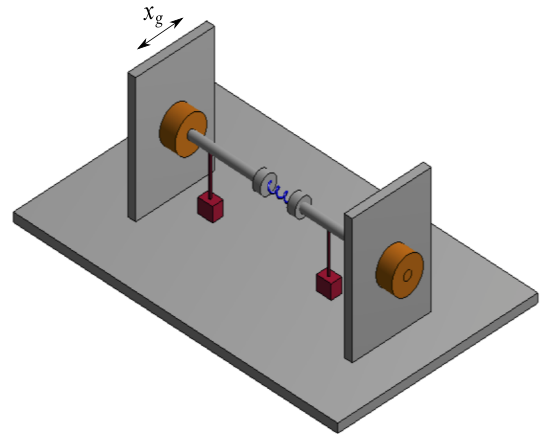
The model used in this paper is based on models validated by physical realizations of coupled pendulums (without harvesters) in the literature (Ikeda et al.[23] and Polczyński et al.[24]). A harvester with a single pendulum and an electromagnetic generator was demonstrated by Ma et al.[25] and Kecik and Mitura.[26] The experimental setup of Ikeda et al.[23] consisted of two disc type pendulums attached to the rotating shafts with a torsional coupling spring. The system was subjected to base excitation by a shaker. A similar coupled pendulum model under electrical pulses was tested by Polczyński et al.[24] with coupled pendulums. The damping induced in experiments is often relatively high, which decreases the amplitude of the response compared to the simulation results.
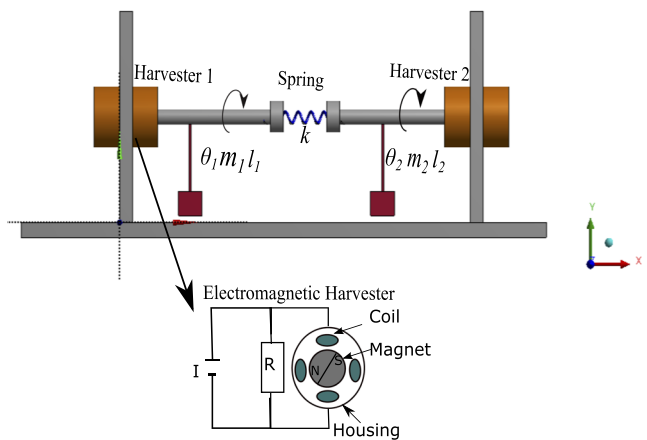
The equations of motion of the pendulums are

$$m_1 l_1^2 \ddot{\theta}_1 + c\dot{\theta}_1 + m_1 g l_1 \sin\theta_1 + k(\theta_1 - \theta_2) - \phi i_1 = -m_1 l_1 \ddot{x}_g \cos\theta_1,$$
$$m_2 l_2^2 \ddot{\theta}_2 + c\dot{\theta}_2 + m_2 g l_2 \sin\theta_2 + k(\theta_2 - \theta_1) - \phi i_2 = -m_2 l_2 \ddot{x}_g \cos\theta_2,$$

$$(1)$$

where $\phi = Bl$, B is the electromagnetic flux, and l is the coil length. Here, the generators for both pendulums are assumed to be identical.

Kirchhoff's voltage law is applied to the electrical circuits, where the coil inductance is L and the load resistance is R for both

(a) Isometric view

(b) Side view and electrical circuit

FIG. 1. Schematic representation of the coupled harvester model.

the circuits. The induced currents i_1 and i_2 are obtained as

$$\phi\dot{\theta}_1 - Ri_1 - L\dot{i}_1 = 0,$$
$$\phi\dot{\theta}_2 - Ri_2 - L\dot{i}_2 = 0.$$

$$(2)$$

To simplify the simulations and improve the physical understandings of the system, the following dimensionless parameters are introduced: normalized time, $\tau = \omega_1 t$ ($\omega_1 = \sqrt{\frac{g}{l_1}}$); normalized current, $I_n = \frac{Li_n}{\phi}$; mass ratio, $\mu_n = \frac{m_n}{m_1}$; length ratio, $\alpha_n = \frac{l_n}{l_1}$; coupling coefficient, $\psi = \frac{\phi^2}{m_1 l_1^2 \omega_1^2 L}$; resistive coefficient, $\zeta = \frac{R}{\omega_1 L}$; mechanical coupling ratio, $\beta = \frac{k}{m_1 l_1^2 \omega_1^2}$; damping ratio, $\gamma = \frac{c}{m_1 \omega_1 l_1^2}$; excitation amplitude ratio, $f = \frac{X_g}{l_1}$ ($x_g = X_g \cos\omega_f t$); and frequency ratio, $\omega = \frac{\omega_f}{\omega_1}$. θ'' and θ' are the non-dimensional acceleration and velocity of the pendulums, respectively. The non-dimensional

electro-mechanical equations are then written as

$$\mu_1 \alpha_1^2 \theta_1'' + \gamma \theta_1' + \alpha_1 \mu_1 \sin \theta_1 + \beta(\theta_1 - \theta_2) - \psi I_1$$
$$= \mu_1 \alpha_1 f \omega^2 \cos \omega \tau \cos \theta_1,$$
$$\mu_2 \alpha_2^2 \theta_2'' + \gamma \theta_2' + \mu_2 \alpha_2 \sin \theta_2 + \beta(\theta_2 - \theta_1) - \psi I_2$$
$$= \mu_2 \alpha_2 f \omega^2 \cos \omega \tau \cos \theta_2, \qquad (3)$$
$$\theta_1' - \zeta I_1 - I_1' = 0,$$
$$\theta_2' - \zeta I_2 - I_2' = 0.$$

Nonlinear equations (3) of the harvesting system are solved numerically using Runge–Kutta integration with a nondimensional frequency step size of 0.01. Parameters $\mu_1 = \mu_2 = 1$, $\psi = 0.1$, $\gamma = 0.03$, $\alpha_1 = 1$, and $f = 0.04$ are kept constant throughout the simulation unless otherwise mentioned. The effect of the mechanical coupling spring on the current generated is shown in Fig. 2. The length ratio $\alpha_2 = 1.04$ is considered, and this introduces mistuning into the system. The mistuning causes the pendulums to harvest the peak power at different frequencies ($\omega = 0.9$ and $\omega = 0.88$ for pendulums 1 and 2, respectively) as shown in Figs. 2(a) and 2(b). $\beta = 0$ indicates uncoupled pendulums. The introduction of the coupling spring (β) converts the pendulums into a two degrees of freedom system giving a bimodal response [peaks (a) and (b) in Fig. 2] for each pendulum. An additional peak (c) is introduced due to the electrical coupling at low coupling ratios. As the coupling ratio increases, the amplitude of the first resonant peak (a) increases by merging with the peak generated by the electrical coupling and the second resonant peak (b) decreases and moves away from the first peak for pendulum 1. However, the peak current generated with coupling is less than that for the uncoupled system. This reduction in current is compensated in pendulum 2 with an increase in both resonant peaks [(a) and (b)]. The increase in the power harvested from pendulum 2 can be attributed to an energy transfer from pendulum 1, which has a higher resonant frequency, to pendulum 2 with a lower resonant frequency. These multiple peaks enhance the possibility to harvest energy at multiple frequencies or from a broadband response.

The effect of the resistive coefficient ζ on the power harvested is shown in Fig. 3. The power harvested in terms of the resistive coefficient has a maximum, where the coupling between the electrical and mechanical systems is optimum.

The introduction of mechanical coupling changes the dynamics of the harvesters. The harmonic balance method is used to understand the dynamics and identify the existence of multiple solutions (refer to the supplementary material for details).

Figure 4 presents the current frequency response of the pendulum harvesters for different coupling ratios β. Blue dots represent the stable solution and unstable regions are represented by red dots. The numerical results are shown by black circles. The soft-spring characteristics in the frequency response curves can be observed with curves bending toward the left. The numerical results are in good agreement with the harmonic balance results.

There are at most seven steady-state solution branches, including four stable [marked as (a)–(d)] and three unstable solutions. High energy orbit solutions, which are not visible through numerical studies, can be observed extending toward the lower frequency zone. This indicates the possibilities of obtaining substantial enhancement in the current magnitude and frequency bandwidth from both pendulums. The existence of low and high energy orbits depends on the initial conditions.

An interesting phenomenon can be observed from the response curves, where an isolated response or frequency island (with stable and unstable parts) coexists with the main response at low excitation frequencies. This type of feature has been observed in coupled nonlinear systems (Alexander and Schilder,[27] Gatti et al.,[28] and Haung et al.[29]), and is often missed in numerical simulations. The existence of these isolated frequency islands depends on the mechanical coupling ratio, and they move away (toward lower frequencies) from the main response with an increase in mechanical coupling. For pendulum 1, the frequency island with a high amplitude coexists with a low amplitude response, whereas an island with a low amplitude coexists with a high amplitude response for pendulum 2.

Different initial conditions (IC) lead to the steady state response occurring on different solution branches, as shown in Fig. 4. To identify the set of initial conditions corresponding to different branches, the basins of attraction for different solutions at two frequencies are shown in Figs. 5(a) and 5(b). The initial conditions of pendulum 2 are varied to obtain these basins, keeping the initial conditions of pendulum 1 as zero ($\theta_1 = 0$ and $\theta_1' = 0$). The initial condition range of pendulum 2 is divided into a 200 × 200 grid. The current output obtained for each set of initial conditions is compared to the different solution branches in Figs. 4(a) and 4(b) and
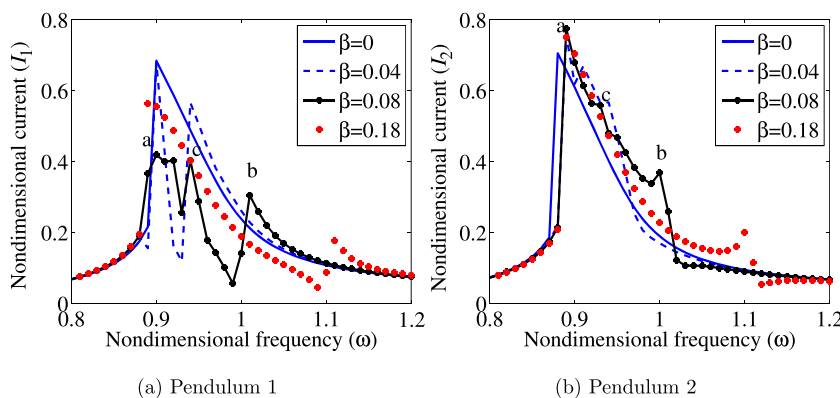

(a) Pendulum 1

(b) Pendulum 2

FIG. 2. Effect of coupling spring (β) on the current generated (rms) showing multiple peaks due to mechanical and electrical coupling, $\zeta = 0.14$ and $f = 0.04$.
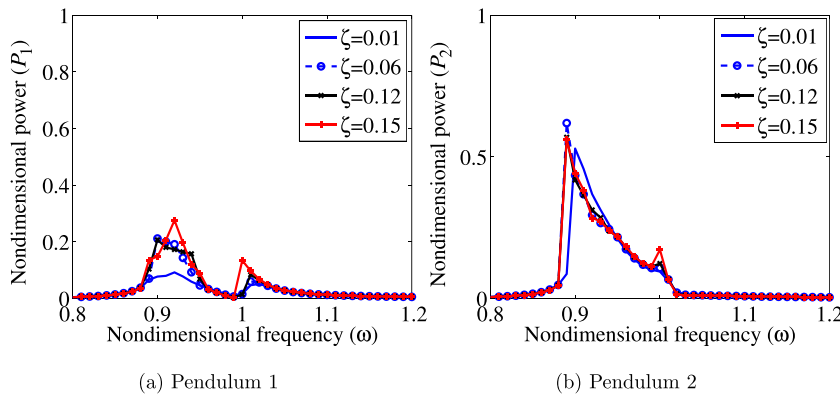
FIG. 3. Effect of resistive coefficient (ζ) on the power generated, β = 0.08.

given a color code. At lower frequencies, solution branch "a" dominates, and only a narrow set of ICs gives solution branch "b," as shown in Fig. 5(a). This indicates a low probability of obtaining the higher energy orbit solution. At higher frequencies (near to the first resonant frequency) the region to obtain the higher energy orbits "b" and "c" enlarges, as shown in Fig. 5(b). Figures 5(c) and 5(d) show the current time histories comparing the outputs from zone "a" (with zero IC) and optimal initial conditions for pendulums 1 and 2

at ω = 0.85. Numerically, instead of the analytic periodic solution "b" [see Figs. 4(a) and 4(b)], a non-periodic (chaotic) solution was obtained, as shown in Figs. 5(c) and 5(d). This solution has an average amplitude between the amplitudes of the "a" and "c" solutions, and consequently is marked by "b" in Figs. 5(a) and 5(b), where the characteristic strange attractor fractal borders can also be seen. Pendulum 2 shows an enhanced current magnitude when the solution belongs to the region with optimal ICs, as shown in Fig. 5(d).
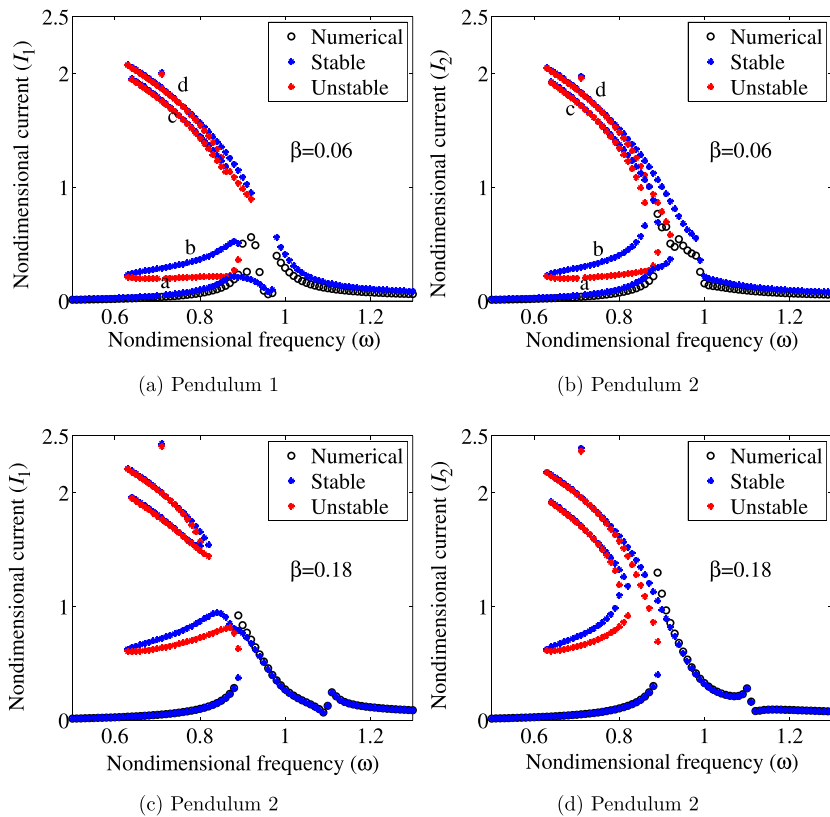

FIG. 4. Results from the harmonic balance analysis and numerical simulations showing different solution branches and frequency islands, ζ = 0.13.
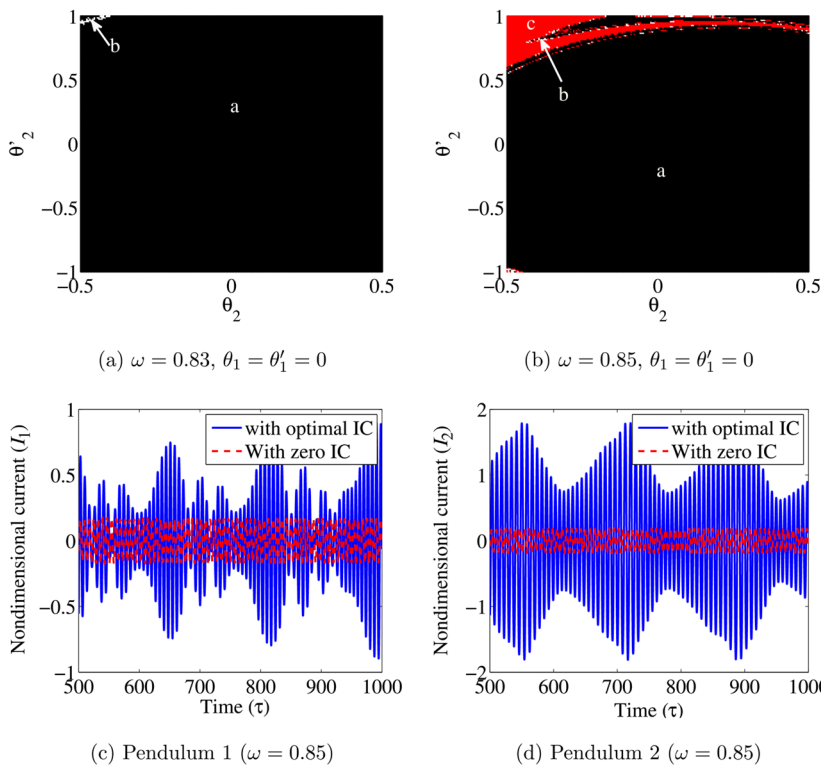
FIG. 5. Basins of attraction and current time histories, for $\theta_2 = -0.3845$ and $\theta'_2 = 0.808$ [black zone-(a), white zone-(b), red zone-(c) correspond to branches in Fig. 4].

Enhancement in harvester performance is shown in Fig. 6. With optimal initial conditions, a huge enhancement of 140% ($d\omega = 0.05$–0.12) in the bandwidth of pendulum 1 can be observed without much enhancement in the peak power. Pendulum 2 shows an enhancement of 11% in the peak power and 54% in the bandwidth ($d\omega = 0.11$–0.17). Ikeda *et al.*[23] reported that the high amplitude branches in the frequency responses can be obtained by the careful choice of initial disturbances. They also observed enhancements in the current generated and bandwidth. The initial energy input to enhance the harvester performance can be realized

physically by a manual method[30] or by chaos control.[31,32] Dehghani and Khanlo[32] proposed a harvester with a tip magnet and external magnets, with adaptive control of the chaotic behavior in the presence of uncertainty.

In summary, this article reports that the performance of the coupled harvester at lower frequencies can be enhanced with a certain set of initial conditions. In practice, this can be achieved by either impact or chaos control. Especially, this design would address the low energy harvesting capability of high frequency harvesters/oscillators. The bandwidth of both harvesters can be
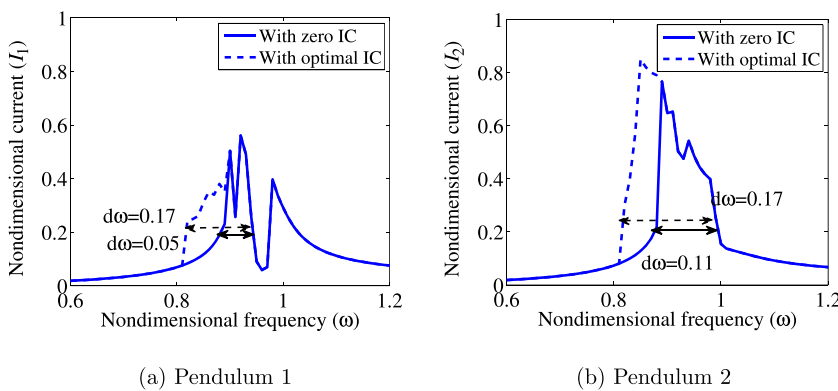

FIG. 6. Bandwidth enhancement with optimal initial conditions, $\zeta = 0.13$ and $\beta = 0.08$.

increased by 140% and 54%, respectively. In addition, a high amplitude frequency island is observed due to the coupling. Possible approaches to obtain these solutions need to be explored.

See the supplementary material for detailed equations.

DATA AVAILABILITY

The data that supports the findings of this study are available within the article.

REFERENCES

[1]S. Roundy, E. S. Leland, J. Baker, E. Carleton, E. Reilly, E. Lai, B. Otis, J. Rabaey, V. Sundararajan, and P. Wright, IEEE Pervasive Comput. **4**, 28 (2005).

[2]D. Castagnetti, Meccanica **54**, 749 (2019).

[3]Y. Li, D. Yin, X. Cheng, J. Chen, A. Zhou, X. Ji, and Y. Li, J. Appl. Phys. **127**, 064104 (2020).

[4]S. F. Ali, M. I. Friswell, and S. Adhikari, Smart Mater. Struct. **19**, 105010 (2010).

[5]M. I. Friswell, S. F. Ali, O. Bilgen, S. Adhikari, A. W. Lees, and G. Litak, J. Intell. Mater. Syst. Struct. **23**, 1505 (2012).

[6]P. V. Malaji and S. F. Ali, Appl. Phys. Lett. **111**, 083901 (2017).

[7]K. Fan, Q. Tan, Y. Zhang, S. Liu, M. Cai, and Y. Zhu, Appl. Phys. Lett. **112**, 123901 (2018).

[8]B. Zhao, J. Wang, J. Liang, and W.-H. Liao, Appl. Phys. Lett. **116**, 063901 (2020).

[9]Y. Zhang, A. Luo, Y. Wang, X. Dai, Y. Lu, and F. Wang, Appl. Phys. Lett. **116**, 053902 (2020).

[10]B. Ambrożkiewicz, G. Litak, and P. Wolszczak, Appl. Sci. **10**, 671 (2020).

[11]V. R. Challa, M. G. Prasad, and F. T. Fisher, Smart Mater. Struct. **18**, 095029 (2009).

[12]A. Erturk, J. M. Renno, and D. J. Inman, J. Intell. Mater. Syst. Struct. **20**, 529 (2009).

[13]B. Yang, C. Lee, W. L. Kee, S.-P. Lim, J. Micro/Nanolithogr., MEMS, MOEMS **9**, 023002 (2010).

[14]P. V. Malaji and S. F. Ali, Eur. Phys. J.: Spec. Top. **224**, 2823 (2015).

[15]J. Chen and Y. Wang, Appl. Phys. Lett. **114**, 053902 (2019).

[16]M. Ferrari, V. Ferrari, M. Guizzetti, D. Marioli, and A. Taroni, Sens. Actuators, A **142**, 329 (2008).

[17]I. Sari, T. Balkan, and H. Kulah, Sens. Actuators, A **145-146**, 405 (2008).

[18]P. V. Malaji and S. F. Ali, Sens. Actuators, A **255**, 1 (2017).

[19]L. Tang and Y. Yang, Appl. Phys. Lett. **101**, 094102 (2012).

[20]Z. Zergoune, N. Kacem, and N. Bouhaddi, Smart Mater. Struct. **28**, 07LT02 (2019).

[21]S. Zhou, J. Cao, W. Wang, S. Liu, and J. Lin, Smart Mater. Struct. **24**, 055008 (2015).

[22]M. Aramaki, T. Yoshimura, S. Murakami, K. Kanda, and N. Fujimura, Appl. Phys. Lett. **114**, 133902 (2019).

[23]T. Ikeda, Y. Harata, and K. Nishimura, J. Comput. Nonlinear Dyn. **10**, 051017 (2015).

[24]K. Polczyński, A. Wijata, J. Awrejcewicz, and G. Wasilewski, Proc. Inst. Mech. Eng., Part I **233**, 441 (2019).

[25]T.-W. Ma, H. Zhang, and N.-S. Xu, Mech. Syst. Signal Process. **28**, 323 (2012).

[26]K. Kecik and A. Mitura, Int. J. Mech. Sci. **174**, 105568 (2020).

[27]N. A. Alexander and F. Schilder, J. Sound Vib. **319**, 445 (2009).

[28]G. Gatti, I. Kovacic, and M. J. Brennan, J. Sound Vib. **329**, 1823 (2010).

[29]D. Huang, S. Zhou, and G. Litak, Nonlinear Dyn. **97**, 663 (2019).

[30]S. Zhou, J. Cao, D. J. Inman, S. Liu, W. Wang, and J. Lin, Appl. Phys. Lett. **106**, 093901 (2015).

[31]K. Aravind, S. F. Ali, and A. Arockiarajan, IFAC **49**, 35 (2016).

[32]R. Dehghani and H. M. Khanlo, J. Vib. Control **25**, 2191 (2019).